PERGAMON

Carbon 40 (2002) 1353–1361

CARBON

Microstructures of PAN-ACF modified by catalytic benzene deposition

An-Hui Lu*, Jing-Tang Zheng

Institute of Coal Chemistry, Chinese Academy of Sciences, P.O. Box 165, Taiyuan 030001, PR China

Received 4 January 2001; accepted 7 November 2001

Abstract

Benzene pyrolysis was successfully introduced to modify the pore size distributions (PSD) of polyacrylonitrile based activated carbon fibers (PAN-ACF) into a sharp distribution, at the presence of nickel catalyst. The microstructures of samples were studied by means of nitrogen adsorption, XRD, and SEM. The nitrogen isotherms were analyzed in detail using the routine BET method, α_s plot, DR equation, Horvath–Kawazoe (HK) equation, and regularized density functional theory (DFT), by which the surface area, micropore volume, and PSD were obtained. The results showed that the pore size of PAN-ACF can be effectively narrowed by catalytic benzene deposition and the PSD showed a unimodal nature, exhibiting potential behavior as a molecular sieve. A fraction residue of catalyst located in the ultramicropores can be washed by acid, resulting in increased BET surface area and micropore volume, which can also be confirmed by XRD and SEM measurements.

Keywords: A. Carbon fibers; B. Chemical vapor deposition; C. Adsorption; D. Microstructure

1. Introduction

Activated carbon fibers (ACF) are usually prepared from PAN fibers, cellulose fibers, phenolic fibers, and pitch fibers by chemical or physical activation [1,2]. As compared with conventional granular or powder activated carbons, ACF have very fast adsorption/desorption rates, and can easily avoid the attrition, channelling and bypass flows arising from the packing of the granular carbon system. Moreover, ACF can be used in the form of cloth, paper or felt. In order to meet with the new applications such as in double layer capacitors [3], catalyst supports [4], and gaseous separation, ACF are expected to have a desired porous structure [5].

It is well known that several methods have been employed to modify the porous structure of carbon, such as selecting proper precursor [6], heat-treatment [7], control of the carbonization/activation conditions [8,9], and chemical vapor deposition (CVD) [10–12]. In the literature, most of the studies have been done on modifying the pore size of activated carbons. For instance, Nguyen [13] modified activated carbon (AC) prepared from macadamia nut shells by benzene deposition, which was capable of separating CS_2 from iso-C_5H_{12}. Hu et al. [14] used 3-methylentane as a carbon source to modify AC with a pore size around 0.5 nm to form a final carbon molecular sieve with pore size 0.33–0.43 nm. Unfortunately, little work has, however, been done on modifying the pore size of ACF [15] as compared with that of AC [16]. It is meaningful to modify and study the microstructure of ACF due to the many advanced features mentioned above, especially, for PAN-ACF, which have been reported to exhibit a high activity for chemical reaction due to their high nitrogen content.

The aim of the current work is to study the microstructures of PAN-ACF modified with a new chemical vapor deposition method using nickel as catalyst. By this method, PAN-ACF can be tailored to have different dominant sizes of pores, enabling them to perform as molecular sieves.

2. Experimental

2.1. Sample preparation

Normal surface area PAN-ACF with specific surface

*Corresponding author.
E-mail address: anhuilu@sxicc.ac.cn (A.-H. Lu).

0008-6223/02/$ – see front matter
PII: S0008-6223(01)00293-7

area 980 m^2/g prepared by steam was termed as ACF1, and high surface area PAN-ACF with 1895 m^2/g prepared by KOH activation was termed as ACF2. Using 2-propanol as solvent, ACF1 and ACF2 were impregnated with nickel nitrate, heated slowly to 393 K and kept for 3–4 h. The percentage of loaded reagent was calculated based on the increase of weight. For ACF1 the catalyst loading was 6%, and for ACF2 it was 8%. The sample was placed in a tubular reactor and then heated under the protection of nitrogen to a final temperature of 973 K. Next, a nitrogen stream containing 3 vol% benzene was introduced into the reactor for 20–40 min, yielding CVD1 and CVD2, respectively, from ACF1; and for 40 min, yielding CVD3 from ACF2. In order to eliminate the diffusion effect as far as possible, a high flow rate of nitrogen (0.02 m^3/h) was chosen. CVD21 was obtained from CVD2 washed by acid.

2.2. Sample characterization

The samples were characterized using low temperature (77.4 K) nitrogen adsorption isotherms measured over a wide range of relative pressure from 10^{-6} to 1. Adsorption measurements were performed on a Micromeritics ASAP 2000 volumetric adsorption apparatus. High purity nitrogen (99.99%) was used. Prior to measurement, the samples were degassed at 573 K for 2 h in the degas pot of the adsorption analyzer.

The nitrogen isotherms were analyzed by high-resolution alpha–s plot analysis [17] and DR equation. The specific surface area of samples was determined from nitrogen adsorption isotherms by the standard BET method [18], micropore surface area and pore volume were obtained from the *t*-plot [18], Dubinin–Astakhov [18] and Horvath–Kawazoe [19] equations. The pore size distribution (PSD) was calculated by employing the regularization method according to density functional theory (DFT) [20].

The X-ray diffraction patterns of PAN-ACF before and after CVD were measured by use of an X-ray diffractometer (XD-3XA Shimadzu Corp). The conditions were as follows: Cu Kα radiation, applied voltage 30 kV, current 30 mA, and scanning angle between 3° and 80°. The SEM photographs of the samples were obtained using a JEM-EX1200 electron microscope.

3. Results and discussion

3.1. Analysis of nitrogen adsorption isotherms

Nitrogen adsorption, because of the relatively small molecular diameter of nitrogen, is frequently used at 77 K to probe porosity and surface area, and also as a standard procedure for characterization of the porous structure of carbonaceous materials. By low-temperature nitrogen adsorption, the porous textural parameters of the original and the corresponding modified samples studied were obtained, as listed in Table 1. After deposition the median pore diameters of CVD1, CVD2, and CVD21 decreased obviously as compared with that of the original ACF1 according to the HK results. The specific surface areas (BET) and micropore volumes of all ACF1 samples studied reduced by 37–47% after deposition, and by acid washing the specific surface area of CVD21 increased by 30% as compared with CVD2. This means that acid washing is an effective method to remove the remaining catalyst in the micropores. In the case of the high surface area ACF2, the specific surface area and pore volume were decreased remarkably by benzene deposition due to the higher catalyst loading as compared with ACF1.

Fig. 1 shows the adsorption isotherms of ACF1, ACF2 and their CVD samples. According to the IUPAC classification [18], the isotherms are of typical type I. There are significant amounts of porosity present in the samples ACF1 and ACF2. Both of the isotherms of ACF1 and ACF2 show a rounded ‘knee’, indicating a wider pore size distribution. After a relative pressure of about 0.1 is reached, there is still a further increase in amount adsorbed with increasing relative pressure, which reflects a certain amount of mesopore volume in ACF1 and ACF2. After deposition the nature of the isotherms for CVD samples shows a difference in the curvature from that of their originals, and the absence of the more rounded ‘knee’, indicating that the pore sizes were narrowed and/or

Table 1
Textural parameters of samples

Sample	S_{BET} ($m^2\ g^{-1}$)	*t*-plot		Horvath–Kawazoe		Dubinin–Astakhov	
		Smi ($m^2\ g^{-1}$)	Vmi (ml g^{-1})	Vmi (ml g^{-1})	Dme (nm)	Smi ($m^2\ g^{-1}$)	Vmi ($m^2\ g^{-1}$)
ACF1	983	782	0.340	0.39	0.56	838	0.332
CVD1	622	534	0.21	0.22	0.49	504	0.192
CVD2	524	452	0.18	0.19	0.48	448	0.170
CVD21	682	582	0.23	0.25	0.48	560	0.212
ACF2	1895	1299	0.56	0.74	0.58	–	
CVD3	291	252	0.10	0.11	0.58	–	
ZSM5	400	366	0.18		0.49	–	

S_{BET}: specific surface area; Smi: micropore surface area; Vmi: micropore volume; Dme: median pore diameter

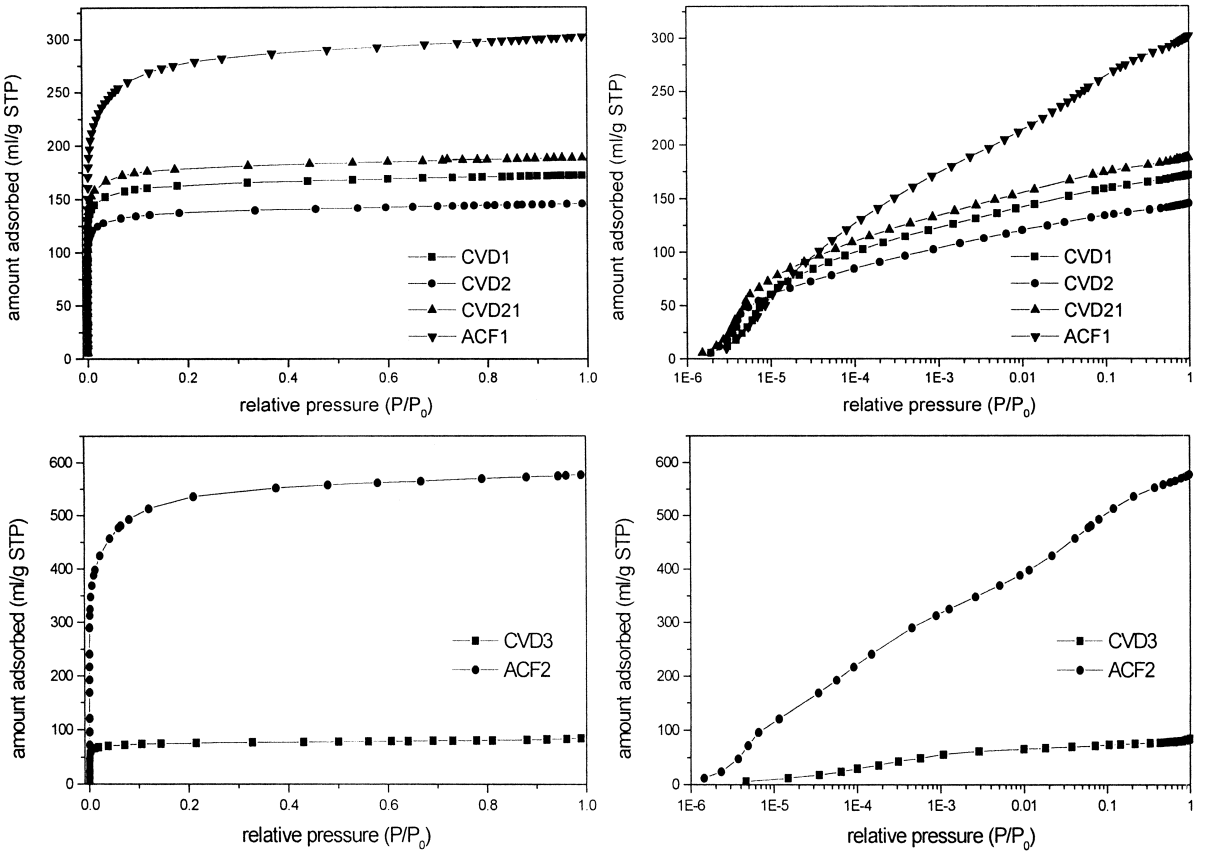

Fig. 1. Nitrogen adsorption isotherms of samples at 77 K.

blocked. All the CVD samples, CVD1, CVD2, CVD21 and CVD3, show a sharp knee and a horizontal plateau, and the amount adsorbed decreased substantially compared to originally. The amount adsorbed decreased to about 172 ml(STP)/g for CVD1, further to 148 ml(STP)/g for CVD2 and to 85 ml(STP)/g for CVD3. Due to a longer deposition time, CVD2 exhibits a lower amount adsorbed than CVD1. After being washed by acid, the amount adsorbed by CVD21 increased to 188 ml(STP)/g, suggesting that the pore volume increases by removing the catalyst in the pores.

A large percentage of the pore filling takes place at relative pressures between 10^{-6} and 10^{-5} for ACF1 and its CVD samples. Beyond that level, the amount adsorbed increases gradually and the isotherms appear to bow away from the *y*-axis. A very interesting change in the nature of the low pressure isotherm is seen in CVD3, where a saturated amount adsorbed has already been reached at relative pressures between 10^{-6} and 10^{-3}, reflecting that most of the pore filling occurs at very low relative pressures and CVD3 is essentially microporous.

Nitrogen adsorption isotherms at low relative pressure have a fine interpretation for the microstructures of PAN-ACF, especially for the micropores adsorption behavior. In the present work, a high resolution α_s-plot was employed to analyze the low pressure adsorption behavior, which was developed by Kaneko and co-workers [17] and was said to be not limited by the submonolayer adsorption; the calculation method has been described elsewhere [21,22]. Nongraphitized carbon black Cabot BP 280 (S_{BET}=40.2 m^2/g) [21] was used as a reference adsorbent. The corresponding parameters, total surface area (S_t), external surface area (S_{ex}), and micropore volume (V_{mi}), calculated from the α_s-plot method are listed in Table 2. It can be seen that the values for S_t, S_{ex}, and V_{mi} of ACF1 and ACF2 decrease after being deposited, which shows a similar trend and good agreement with the results listed in Table 1. As expected, the porous structures of PAN-ACF can be modified by catalytic benzene deposition.

The high resolution α_s-plots of ACF1, ACF2, and their CVD samples are shown in Fig. 2. All of them exhibit a filling swing in the low pressure region (α_s<0.5) and an almost linear part at α_s>1, reflecting that the adsorption on the ACF and CVD samples is different from that on the flat surface, which arises from the enhancement of adsorption by the micropore field. The plots of CVD1,

Table 2
Total surface area S_{total}, external surface area S_{ex}, and micropore volume V_{mi} calculated from α_s-plots

Sample	α_s-plot		
	S_{total} (m^2g^{-1})	S_{ex} (m^2g^{-1})	V_{mi} (cm^3g^{-1})
ACF1	1060	25.3	0.46
CVD1	712	4.6	0.26
CVD2	590	3.2	0.22
CVD21	725	5.4	0.28
ACF2	2195	18.6	0.86
CVD3	390	4.4	0.12

CVD2, and CVD21 are very similar except for the amount adsorbed. A longer deposition time gives CVD2 a lower amount adsorbed than that by CVD1, and the amount adsorbed by CVD21 increases substantially by acid washing. The filling swing suggests empirically the presence of micropores whose width is less than 1.0 nm [22]. Especially, it can be seen that CVD1, CVD2, and CVD21 show a remarkable filling swing as compared with ACF1 and ACF2, indicating that deposited carbon narrows or blocks the pore mouth of ACF1 and ACF2 effectively. The filling swing for CVD samples at $\alpha_s<0.5$ corresponding to relative pressure below $P/P_0 = 0.01$ probably corresponds to a pronounced molecule sieve effect. This should be associated with the 'primary micropore filling' proposed by Gregg and Sing [18]. In these pores, the interaction between pore wall and molecule is noticeably enhanced due to the overlapping of the potential from the opposite pore walls [23], to provide a marked upward deviation at the low α_s region. In the case of CVD3, higher catalyst loading compared with CVD2 corresponds to the special filling swing, which becomes much flatter and highly coincident with the dot line and quite differs from those of other CVD samples. The special plot at $\alpha_s<0.5$ indicates the size of pores should be larger and more concentrated than that of the others.

It is necessary to synthesize the nitrogen adsorption data acquired from different analytical methods in order to describe the true adsorption process on microporous solids. The DR equation gives a mathematical description of the micropore filling process, which is said to be applicable to microporous solids. The DR equation: $W = W_0 \exp[-(A\beta/$

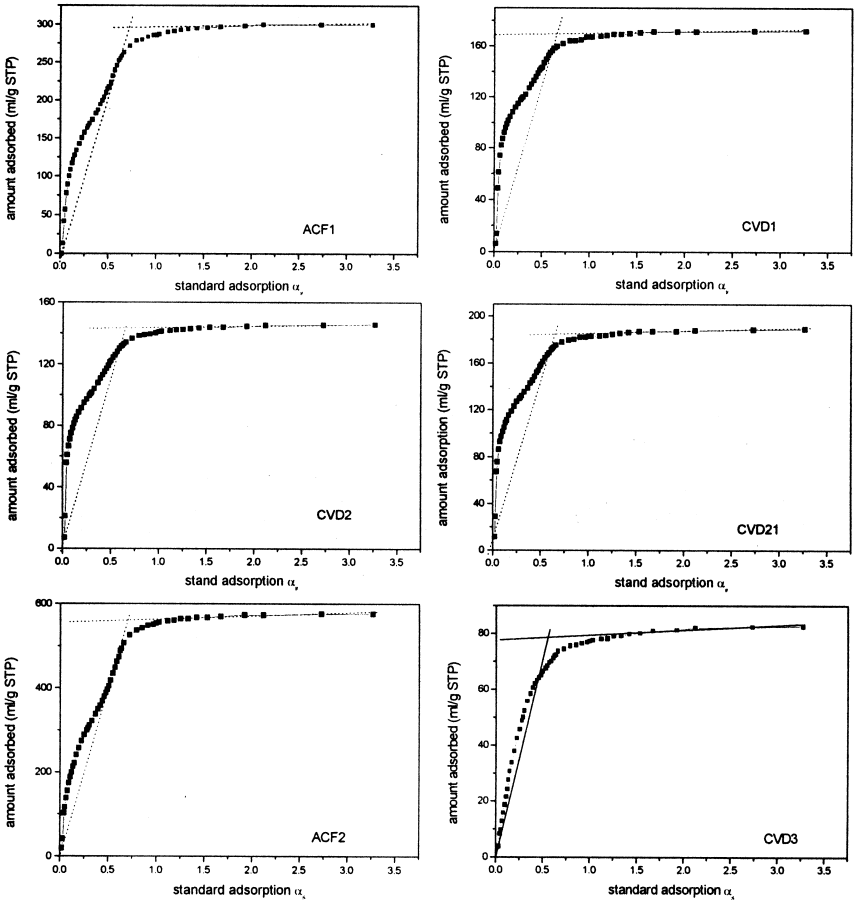

Fig. 2. High resolution α_s-plots for samples under study.

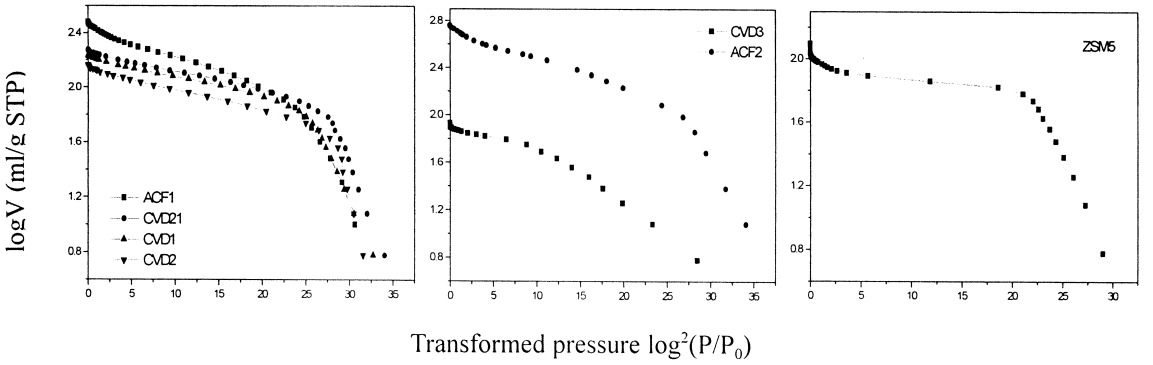

Fig. 3. DR plots for the nitrogen adsorption of samples at 77.4 K.

$E_0)^2$], where W is the amount of gas adsorbed at temperature T, and relative pressure P/P_0, W_0 is the micropore volume, $A = RT\ln(P/P_0)$ is the adsorption potential, and R is the gas constant; E_0 is related to the adsorbent, $E = \beta E_0$ is an energy constant which can be factorized in a characteristic adsorption energy, the affinity coefficient β represents the ratio of the characteristic adsorption energies of the test and reference vapors. Dubinin and Stoeckli [24] suggested the relationship between the characteristic adsorption energy and the average half-width, x, of the slit-like pores, $x = K/E_0$. Usually, the affinity coefficient of nitrogen is $\beta = 0.33$. For molecular sieve adsorbents, the average value of K is 10 kJ nm mol^{-1}, and the characteristic energies, E_m, are in the range of 28.5–35.6 kJ mol^{-1} [24].

In the present study, ZSM5 (textural parameters listed in Table 1) was also presented and its DR plot was also investigated for comparison purpose. As can be seen in Fig. 3, the DR plots of ACF1, ACF2 and ZSM5 can be divided into the first, second, and third stage in order of increasing relative pressure, however, those of CVD samples show approximately two stages. All DR plots exhibit negative deviations occurring at the first stage. It can be seen that longer CVD time makes the slope of the first stage of ACF1 be sharper and move to a lower relative pressure as seen in CVD2, furthermore, the sample CVD21 washed by acid also shows the same trend. However, the slope of the second stage becomes more horizontal than that of ACF1. The very special DR curve of CVD3 has a longer first stage than any other, which may be due to the absence of the ultramicropores.

The parameters, adsorption energy and half-width, for samples under study are calculated by the multistage micropore filling mechanism [25], and are listed in Table 3. The E_{01} of the first stage is smaller than that of the other stages and the x_1 of the first stage shows a contrary trend. Therefore, nitrogen molecules can easily diffuse into pores according to the x_1 which is bigger than the critical size of pores that nitrogen molecules can enter into [23]. However, to some extent, we propose that the first stage, i.e, the negative deviation, does not ascribe to the active diffusion effect proposed by the carbon scientists [26]. In our opinion, the high-energy defect sites on the external surface of ACF such as steps or ridges, would cause strong specific interactions with the quadrupole of nitrogen molecule [27] and probably enhance the adsorption in the low relative pressure and result in a big x_1 value.

The deposition process gives the CVD samples a higher E_{02} and a smaller x_2 value. Comparing the E_{02} with E_m [24], and combining the x_2 with the mean diameter obtained by HK results, it can be concluded that the second stage of CVD samples exhibits significant molecular sieve behavior. Thus, a molecular sieve type PAN-ACF can be successfully prepared by catalytic chemical vapor deposi-

Table 3
Adsorption energy E_0 and half-width x of samples obtained by DR equation

Sample	E_{01} (kJ mol^{-1})	X_1 (nm)	R_1^2	E_{02} (kJ mol^{-1})	X_2 (nm)	R_2^2	E_{03} (kJ mol^{-1})	X_3 (nm)	R_3^2
ACF1	8.96	1.12	0.974	20.53	0.49	0.996	14.38	0.70	0.996
CVD1	7.81	1.28	0.999	24.04	0.42	0.997	–	–	–
CVD2	5.65	1.77	0.997	22.9	0.44	0.996	–	–	–
CVD21	7.25	1.38	0.997	23.68	0.42	0.989	–	–	–
ACF2	8.25	1.21	0.999	19.12	0.52	0.993	13.28	0.75	0.999
CVD3	12.98	0.77	0.997	24.45	0.41	0.995	–	–	–
ZSM5	8.00	1.25	0.996	38.69	0.26	0.998	14.13	0.71	0.990

tion. The lower E_{02} of CVD samples is close to (but less than) E_m [24], which may be attributed to the rapid adsorption/desorption rates caused by the micropores developed on surface of the fibers.

3.2. PSD of sample before and after CVD

The thermodynamic behavior of a fluid, or a fluid mixture, adsorbed in an ACF depends principally on its PSD. Characterization of the PSD is therefore an important problem in an application involving the use of ACF. As reported, in the case of low temperature nitrogen adsorption the HK method works reasonably well for samples which possess essentially small micropores (width below about 0.9 nm) and small external surface area [21]. Therefore, we employ HK method [19] to analyze the micropore size distributions of samples before and after CVD.

It can be seen in Fig. 4 that all samples showed an unimodal PSD except ACF2. After the CVD process, the PSDs of CVD1, CVD2 and CVD21 become sharper and narrower than that of the original ACF1. The different degree of deposition has contributed to a slightly different PSD between CVD1 and CVD2 and a longer period of deposition contributes to the pore-size of CVD2 decreasing obviously from 0.56 to 0.48 nm, which exhibits a distinct property of molecular sieve. So normal surface area PAN-ACF can be modified to have a narrow range of pore size by benzene deposition in the presence of catalyst at a suitable condition. After being washed by acid, the PSD of CVD21 keeps a similar shape to that of CVD2. However, the pore volume increases due to the greater volume released by dissolving catalyst located in the micropores, as is confirmed by the results obtained from the *t*-plot, HK and DA methods as seen in Table 1. In the case of CVD3, deposited carbon blocks significantly the ultramicropores

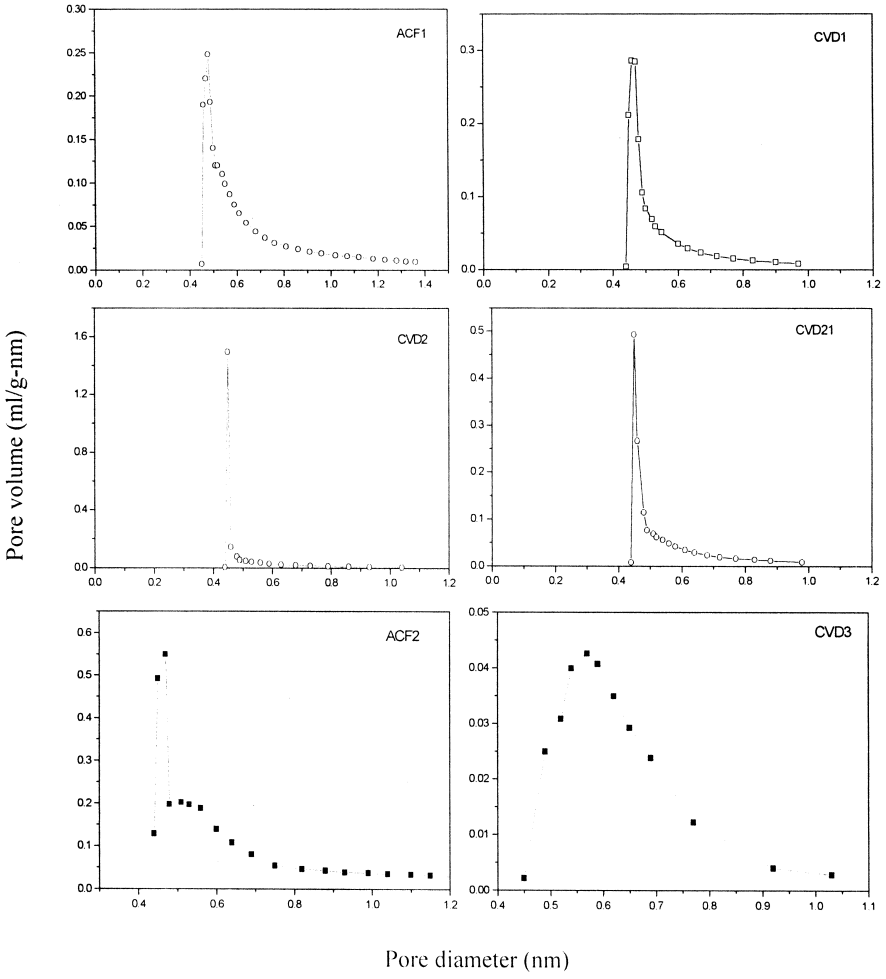

Fig. 4. Micropore size distributions of samples by H–K method.

around 0.5 nm and results in the pore volume decreasing strikingly as compared with the original ACF2, and makes the pores locate at around 0.58 nm.

Being different from the HK method for micropores, the DFT pore-filling model describes adsorption over the entire range of carbon pore sizes, which could accurately describe the density profile of the inhomogeneous adsorbed fluid within carbon slit pores [28]. Through interpretation of the nitrogen adsorption data, the whole PSD of samples studied is generally determined by the DFT method. As shown in Fig. 5, a broad distribution of pore size is evident in the original samples ACF1 and ACF2 and a certain volume of pores in the mesoporous range can be seen clearly. The pores in the range of 2–5 nm are attributed to the slight increment during further adsorption in the isotherms. As expected, the PSD of ACF1 was narrowed and the size of the pore larger than 1.0 nm was blocked significantly in the case of CVD1 and a sharp peak occurred at around 0.73 nm. With increasing deposition time, the pore size becomes narrower and concentrates around 0.7 nm for CVD2. There is a clear difference between CVD2 and CVD21 at the pore size around 0.6 nm, which were raised by acid washing, but the size of pore larger than 1.0 nm remains unchanged. Therefore, it can be inferred that the catalyst mainly exists in the ultramicropores. The dissolving of the catalyst located on the external surface will not affect the final PSD of CVD21. In the case of CVD3, it is very interesting that the PSD is unimodal and the dominant pores are around 0.9–1.0 nm and the pores in the range 0.5–0.9 nm and 1.0–5.0 nm are blocked strikingly, resulting in a lower adsorption capacity than that of the original ACF2. According to the data listed in Tables 1 and 2, it can be inferred that higher nickel content contributes to the extreme influence on the deposition of ACF2 as compared with ACF1, causing the external surface, ultramicroporous and mesoporous volume to be greatly reduced. This is the reason that why CVD3 is so special as discussed above in the α_s plot and DR equation. In brief, the calculated PSDs support well the conclusion drawn from the above examination of their adsorption isotherms.

In order to have an insight into the deposition mechanism, the benzene deposition process is discussed on the basis of the above analysis. As it is known that, the diameter of Ni^{2+} and NO_3^- is 0.15 and 0.2 nm [29,30], respectively. Therefore, nickel-nitrates cannot enter into ultramicropores less than 0.55 nm, but can enter into the big micropores and mesopores easily in PAN-ACF according to the nitrogen isotherm analysis. During the deposition process, benzene molecules preferentially deposit on the accessible region for diffusion reasons, i.e., the metallic nickel particles being on big micropores and the external surface of ACF cause the pore mouth (pore width larger than 1.0 nm) to be blocked and/or narrowed down. Hence the nickel catalyst in the inner part of the pores will be inaccessible for benzene molecules due to the blockage of the pore mouth and the accelerated deposition at the pore mouth in the presence of catalyst. Thus the remaining

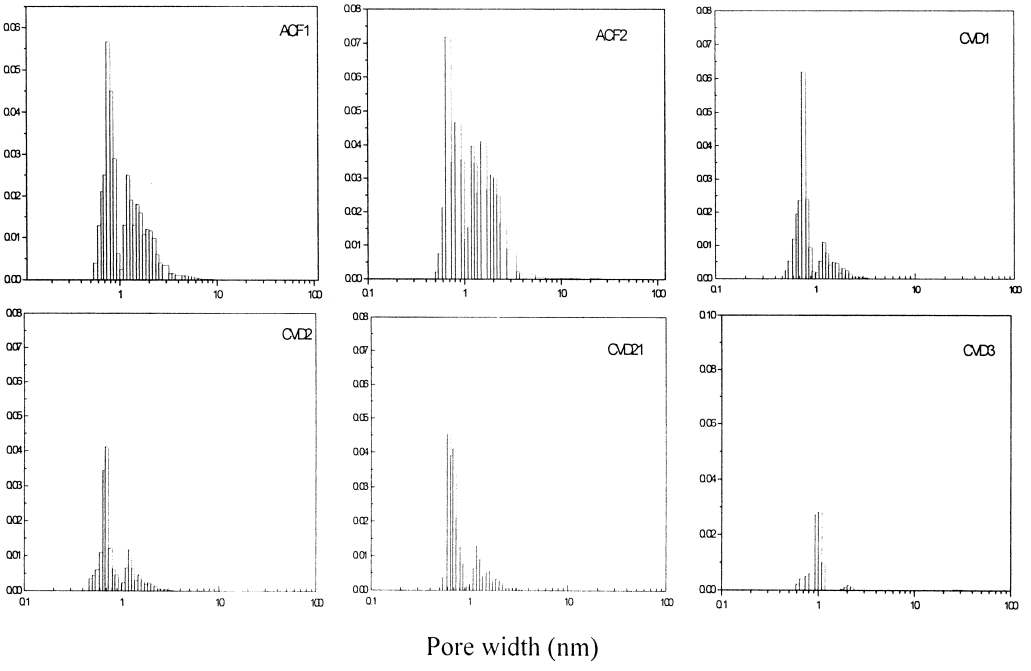

Fig. 5. Pore size distributions of samples by DFT method.

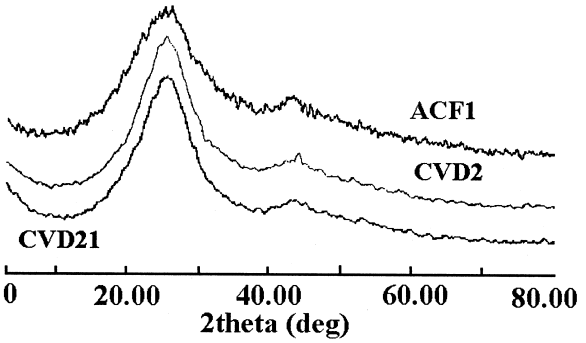

Fig. 6. XRD patterns of samples.

catalyst could be dissolved by acid in the case of CVD21, which results in the occurrence of the pore around 0.6 nm and the increase of pore volume, as seen in Figs. 1 and 5. On the other hand, benzene molecules were easily captured and deposited on the ultramicropore mouths, causing blockage of pores with width 0.5–0.7 nm. That can be ascribed to the following reasons: the overlapping of the potentials from the opposite pore wall [23] causing high adsorption capacity of ACF at low benzene vapor concentration [31], as well as the presence of catalyst in ultramicropores. Higher catalyst loading is very sensitive to blocking pores larger than 1.0 nm by deposited carbon.

3.3. XRD and SEM

To gain a further insight into the deposition process, the selected samples, ACF1, CVD2 and CVD21, were characterized by X-ray diffraction. As seen in Fig. 6, the broad diffraction peaks of ACF1 indicate a disorder amorphous material. The diffraction angles are 25.7° and 43.3°, which are assigned to 002 and 10 peaks, respectively [32]. For CVD2, the small sharp angle at 44.3° overlapping with that of ACF1 is ascribed to the nickel oxide [16] peak, which may be caused from fine metallic nickel oxidized by the air. The lower intensity of the NiO peak occurring on the XRD pattern was due to the lower content of NiO loaded on ACF1. After being washed by acid, the NiO peak 44.3° disappears, which agrees well with the HK, DFT and other analysis methods.

Furthermore, the external surface ACF2 before and after CVD are observed using SEM, as shown in Fig. 7. It can be seen that not only the nickel particles but also the grown whiskers can be observed clearly, and the external surface becomes rather coarse after deposition. Although detail of the pore blocking and/or narrowing cannot be seen by SEM directly, it still might be inferred that catalytic chemical vapor deposition is a feasible means to modify microstructures of PAN-ACF in the presence of catalyst, as discussed above.

4. Conclusions

Normal and high surface area PAN-ACF can be effectively modified to exhibit a unimodal pore size distribution by catalytic benzene deposition, and the dominant pore is around 0.6–0.7 nm for normal surface area ACF and 0.9–0.1 nm for high surface area ACF according to DFT results. The bigger pores are preferentially blocked or narrowed, and the deposition process is probably accelerated and enhanced in the presence of catalyst. The modified PAN-ACF is expected to exhibit the property of molecular sieves for its narrower PSD.

Acknowledgements

This work was financially supported by the National Natural Science Foundation of People's Republic of China

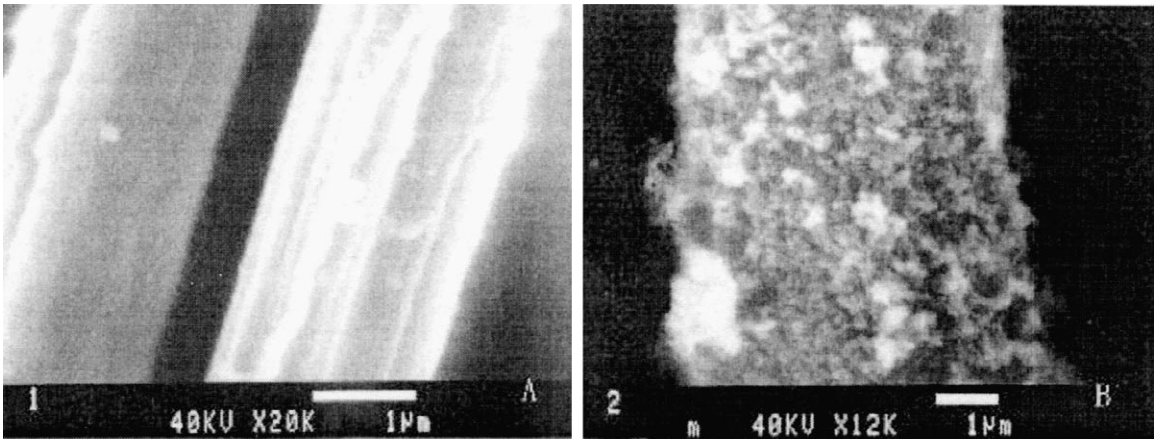

Fig. 7. SEM images of ACF2 (A) and CVD3 (B).

(No. 59672025). The authors would also like to thank the reviewers for many helpful suggestions to improve the clarity of presentation.

References

[1] Stoeckli F, Daguerre E, Guillot A. Carbon 1999;37:2075–7.
[2] Thwaites MW, McEnaney B, Botha FD et al. Preprints Division of Fuel Chemistry of ACS 1992;37(2):497–504.
[3] Tanahashi I, Yoshida A, Nishino A. Carbon 1990;28:477–82.
[4] Imai J, Souma M, Oaeki S et al. J Phys Chem 1991;95:9955–60.
[5] Oya A, Yashida S, Abe Y et al. Carbon 1993;31:71–3.
[6] Oya A, Yoshida S, Alcainz-Monge J et al. Carbon 1995;33:1085–90.
[7] Lizzio AA, Rostam-Abadi M. Carbon 1993;34:97–122.
[8] Miura K, Nakagawa H, Kawano T. TANSO 1998;185:249–55.
[9] Nakagawa H, Watanabe K, Harada Y et al. Carbon 1999;37:1455–61.
[10] Cabrera AL, Zehner JE, Coe CG et al. Carbon 1993;31(6):969–76.
[11] Manso R, Centeno TA, Pajares JA. In: Eurocarbon '98, Strasbourg France, 1998, pp. 729–30.
[12] De Salaza CG, Speulveda-Escribano A, Rodriguez-Reinoso F. In: 24th Carbon Conference, 1999, pp. 36–7.
[13] Nguyen C, Do DD. Carbon 1995;33:1717–25.
[14] Zhonghua Hu, Vansant EF. Carbon 1995;33:561–7.
[15] Kawabuchi Y, Masahiso K, Kawano S et al. Langmuir 1996;12(17):4281–5.
[16] Wang S, Lu GQ. Carbon 1997;36:283–92.
[17] Setoyama N, Suzuki T, Kaneko K. Carbon 1998;36(10):1459–67.
[18] Gregg SJ, Sing KSW. Adsorption, surface area and porosity, 2nd ed. London: Academic Press, 1982.
[19] Horvath G, Kawazoe K. J Chem Eng Japan 1983;16(8):470–5.
[20] Kruk M, Jaroniec M, Bereznitski Y. J Colloid Interf Sci 1996;182:282–8.
[21] Kruk M, Jaronec M, Gadkaree PK. J Colloid Interf Sci 1997;192:250–6.
[22] Kruk M, Jaronec M, Choma J. Carbon 1998;36(10):1447–58.
[23] McEnaney B. Carbon 1988;26(3):267–74.
[24] Dubinin MM, Stoeckli HF. J Colloid Interf Sci 1980;75(1):34–42.
[25] Kakei K, Ozeki S, Suzuki T et al. J Chem Soc Faraday Trans 1990;86(2):371–6.
[26] Marsh H. Carbon 1987;25(1):49–58.
[27] Quirke N, Tennison SRR. Carbon 1996;34(10):1281–6.
[28] Dombrowski RJ, Hyduke DR, Lastoskie CM. Langmuir 2000;16:5041–50.
[29] Coenen JWE. Appl Catal 1991;75:193–223.
[30] Yao T, Xie Y, Gao Y. In: Physical chemistry manual, China: Shanghai Science Technology Publishing House, 1985, pp. 102–32.
[31] Daley MA, Tandon D, Economy J et al. Carbon 1996;34(10):1191–200.
[32] Short MA, Walker Jr. PL. Carbon 1963;1:3–9.